On Scene-Adapted Illumination Techniques for Industrial Inspection

Robin Gruna
Vision and Fusion Laboratory
Karlsruhe Institute of Technology (KIT), Germany
Email: robin.gruna@kit.edu

Jürgen Beyerer
Fraunhofer Institute of Optronics, System Technologies and Image Exploitation (IOSB), Germany
Email: juergen.beyerer@iosb.fraunhofer.de

***Abstract*—In many machine vision applications for automated inspection the illumination design is crucial to the robustness and speed of the inspection process. Hence, there is need to investigate and to experimentally evaluate new illumination designs and techniques. We briefly review a representative selection of illumination techniques that aim to minimize the effort of defect detection by adapting the illuminating light field to the nominal state of the inspection task. Based on this principle we propose an illumination technique using a projector-camera system which provides inspection images that directly display differences in the reflectance between two scenes. A comparison with image differencing for deviation detection shows that the proposed illumination technique is in many cases advantageous from a signal-to-noise point of view.**

I. Introduction

The choice of an appropriate illumination design is one of the most important steps in creating successful machine vision systems for automated inspection tasks. Since in image acquisition all information about a scene is encoded in its exitant light field, the incident light field provided by the illumination must be able to reveal information relevant to the inspection task about the test object. Moreover, in real-time machine vision applications where time is a major constraint, appropriate illumination can greatly simplify digital image processing tasks and improve their processing time and reliability. For instance, an illumination that results in images with high contrast between object and background, simple image thresholding may suffice for object segmentation and more sophisticated and time consuming algorithms can be avoided.

While there are well-founded design rules for choosing the imaging optics for a machine vision system [1], rules for illumination design are less elaborated. However, one general design objective is to provide an illumination that accentuates the features of interest, such as surface defects of a faulty test object, while it minimizes distracting features, e.g., flawless object regions. Some popular illumination techniques like dark-field illumination [2] and techniques based on polarized light [3] explicitly take care of this demand. In dark-field illumination, a directional illumination is used to enhance the visibility of surface features like scratches or indentations on an otherwise smooth surface. In the presence of a perfectly smooth surface, which is assumed to be the desired nominal state of the inspection task, all incident light is reflected away from the camera's lens and the captured image is dark. Imperfections on the surface scatter light into the lens and appear as bright image features. Similarly, in a illumination setup where a polarized illumination (*polarizer*) is used in combination with a crossed polarizing light filter in front of the camera (*analyzer*), object features with polarizing properties can be highlighted. Viewing the test object in its desired nominal state where it is assumed that no change in polarisation occurs, the light received by the camera is almost completely attenuated by the analyzer and thus a dark inspection image is captured. However, object features that cause a rotation in the angle of polarization, like unwanted refractive index variations or stress in transparent objects, are captured as bright image features. The principle behind both illumination techniques is to generate inspection images that highlight deviations from a predefined desired nominal state with high contrast.

Recently, some novel inspection methods have been proposed that take the aforementioned principle a step further by employing more sophisticated illumination techniques. Techniques like inverse fringe projection [4][5], inverse patterns for deflectometric inspection [6] and comparative digital holography [7] are able to directly highlight differences in the shape of two objects. Defect detection by comparing the actual state of a test object with the desired nominal state of a master object is a standard task in industrial inspection. In the case of fringe projection and deflectometry, the shape information of a preceding measurement is used to compute an inverse structured light pattern of the master object which is then used to evaluate a test object. If master and test object are identical, a predefined undistorted pattern is obtained. Otherwise, shape differences are directly highlighted by local geometric distortions in the projected pattern. In the case of holography techniques for object comparison, the coherent optical wave field of the master object is obtained by digital holography. By illuminating the test object with the coherent mask of the master object, differences in the shape between the two objects are directly displayed in the inspection image.

All the described inspection techniques have in common that the illuminating light field is adapted to the desired nominal state of the inspection task. Hence, the captured inspection images directly highlight deviations from the nominal state and therefore reduce the effort of defect detection through digital image or signal processing. This means that feature

978-1-4244-2833-5/10/$25.00 ©2010 IEEE

extraction for defect detection partly takes place in the optical domain, that is, during image formation. We believe that this illumination principle is a promising technique for fast and robust industrial inspection tasks and is worth to be investigated in more detail.

In this article, we apply this principle to propose an illumination technique that is designed to highlight differences in reflectance of two scenes. Our goal is to provide a spatially adapted illumination pattern that results in a featureless constant gray inspection image if the illuminated test object is identical to the master object. However, differences in reflectance of the two objects, e.g., caused by defects, should result in detectable image features that highlight the faulty areas. This goal is achieved by utilizing a digital light projector as light source and a technique referred to as *radiometric compensation* in the literature [8].

In the following sections, we describe the setup of a projector-camera system that is able to generate such illumination patterns and explain the radiometric compensation method used in our experiments. Furthermore, experimental results are presented and the advantages of the proposed illumination technique compared to conventional techniques for deviation detection are discussed. In the following, the adapted illumination pattern that results in a constant gray camera image is referred to as the *inverse illumination mask* of a scene.

II. Inspection Image Acquisition by Means of Inverse Illumination

In recent years, digital video projectors gained great interest in the computer vision and graphics community due to enormous technological advancements such as higher spatial resolution and dynamic range [9][10][11]. Since the radiance of each projector pixel can be controlled separately, they are therefore ideally suited as experimental platforms for evaluating new illumination techniques. In combination with a light sensing device such as a camera, systems that utilize digital video projectors as controllable illumination are referred to as *projector-camera systems* in the literature. Projector-camera systems allow to project arbitrary complex illumination patterns onto a scene and to capture the corresponding images. These optically coded images allow computing information about the scene which is not possible to be retrieved with standard illumination techniques.

Computing the inverse illumination mask of a scene is closely related to the problem of radiometric compensation, which has been widely discussed in the field of projector-camera systems [8][12][13]. Radiometric compensation deals with the problem of displaying projected images on arbitrary surfaces with varying color, reflectance and geometry. When an image is projected onto such a non-cooperative surface, the appearance of the image is modulated by the spatially varying reflectance and distorted by geometric variations. To be able to preserve the original intended appearance of the projected image, a camera serves as a proxy for the human viewer and provides information on how the projected image has to be

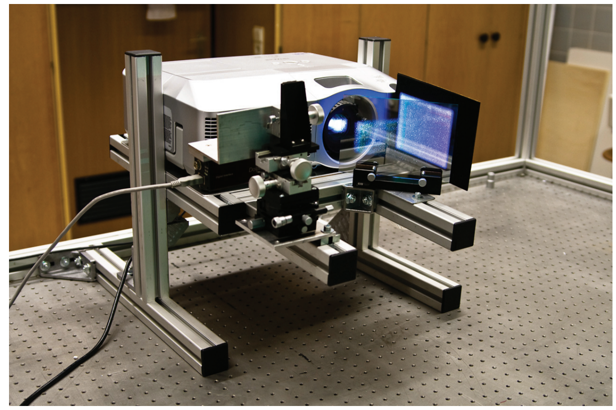

(a) Prototype system

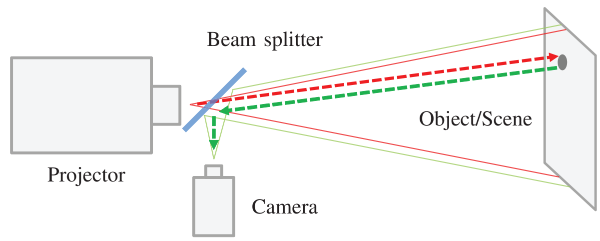

(b) Scheme of a coaxial projector-camera system

Fig. 1. A coaxial projector-camera system.

compensated prior to projection in order to account for the aforementioned perturbations. For our purposes, radiometric compensation is used to compute the compensated constant gray image for a certain test scene. Then, the compensated image is exactly the inverse illumination mask that has to be projected onto the scene in order to capture a constant gray inspection image.

A. Projector-Camera Correspondence

For radiometric compensation a precise mapping between camera and projector pixels has to be established. To avoid parallax errors, a coaxial projector-camera setup, as proposed in [14], is chosen. As shown in Figure 1, a beam-splitter is put in front of both the camera and the projector optics. In addition, the camera is attached to an assembly of mechanical positioners, which allows a precise linear and angular positioning of the camera. By a manual calibration procedure, both centers of field of view are aligned so that a scene-independent viewing geometry is obtained.

However, a pixel-wise alignment can not be established in a purely optical manner. Hence, a geometrical mapping between points $\mathbf{x}_p = (u_p, v_p)$ in the projected image and points $\mathbf{x}_c = (u_c, v_c)$ in the captured camera image is introduced. For this purpose, piecewise second-order polynomials for modeling this mapping are used as proposed in [8]. The polynomial model for each piece of the image domain can be written as

$$\mathbf{x}_p = \mathbf{A}\hat{\mathbf{x}}_c, \text{ where } \hat{\mathbf{x}}_c = (u_c^2, v_c^2, u_c v_c, u_c, v_c, 1)^T, \quad (1)$$

and where the matrix $\mathbf{A} \in \mathbb{R}^{2\times 6}$ contains the unknown coefficients for the mapping. These coefficient are computed by the least-squares-error fitting method using corresponding points from camera and projector images. Corresponding point pairs are obtained by projecting and capturing a sequence of binary coded markers, which are then extracted by image thresholding and connected component analysis.

With (1), for each camera pixel the corresponding projector pixel can be determined. However, the calculated pixel positions usually do not fall into the integer grid of the input image of the projector. Hence, the value of each projector pixel has to be determined by interpolation, taking neighboring pixel values into account. Due to the well known problems of geometric forward image transformations, backward transformation is used to geometrically transform and resample the image prior to projection. The needed inverse geometric mapping is obtained by swapping input and output points and fitting the polynomial model as described above. When the geometric backward transformation is applied to an input image, the projected image appears undistorted to the camera and the captured image matches with the original image in nearly pixel-wise manner.

B. Error-Feedback Approach To Radiometric Compensation

Most approaches to radiometric compensation found in the literature are based on the inversion of a radiometric model that describes the image formation in a projector-camera system via a projection screen with spatially varying reflectance [8][15][16][13]. The model parameters for a static scene are computed by projecting and capturing a set of calibration images. This allows to compensate arbitrary images prior to projecting onto the same static scene. However, when the scene changes, all model parameters have to be recomputed. Since the calibration procedure is computationally demanding, the model based approach is impractical and time-consuming when experimenting with varying scenes and objects.

In [14] and [8], a method for radiometric compensation using the error between the desired and measured appearance of the projected image is proposed. The appearance of the projected image is continually measured by the camera and the computed error is used to adapt the projected image to meet the desired appearance. Let $g_{target}(\mathbf{x})$ be the desired original image and $g^t_{ms}(\mathbf{x})$ the corresponding measured image when $g^t_{proj}(\mathbf{x})$ is projected. At $t = 0$, the algorithm starts by projecting $g^0_{proj}(\mathbf{x}) := g_{target}(\mathbf{x})$. Then the adapted compensation image for time $t+1$ is computed by

$$g^{t+1}_{proj}(\mathbf{x}) := g^t_{proj}(\mathbf{x}) + \gamma(g^t_{ms}(\mathbf{x}) - g_{target}(\mathbf{x})) \ , \qquad (2)$$

where $\gamma \in (0,1)$ is a gain factor and addition is defined component-wise for each color channel separately. By setting $g_{target}(\mathbf{x}) = k$ to a constant gray value k and let the error-feedback algorithm converge to a small constant error, $g^t_{proj}(\mathbf{x})$ becomes the inverse illumination mask and the measured image $g^t_{ms}(\mathbf{x})$ approaches $g_{target}(\mathbf{x})$. Typically, the algorithm converges after a few iterations t (see Figure 2d) and is therefore ideal for experimenting with varying scenes.

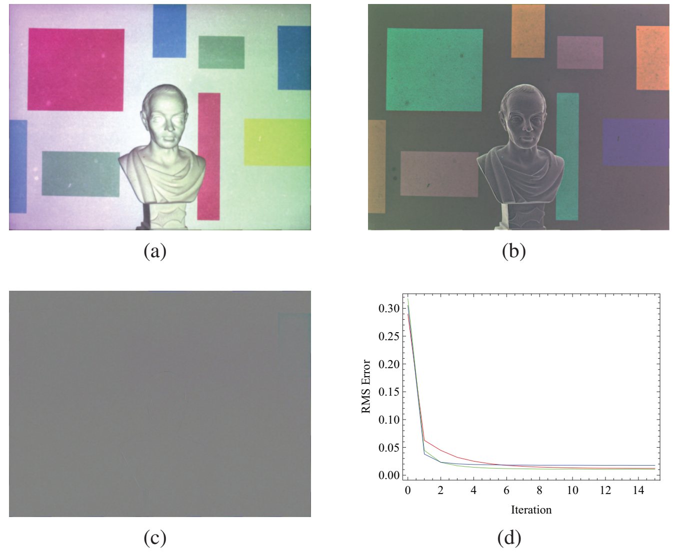

Fig. 2. Experimental results of the error-feedback algorithm. (a) Image of test scene when a constant gray image is projected. (b) Inverse illumination mask computed by the error-feedback algorithm. (c) Measured camera image when the inverse illumination mask is projected onto the scene. (d) RMS error between desired constant gray image and actually measured camera image for each iteration of the error-feedback algorithm (red, green and blue indicate the error for each color channel).

III. Experimental Results

The error-feedback method presented in Section II-B is utilized to compute the inverse illumination mask of a test scene. Figure 2 summarizes the results obtained for a scene that consists of a flat colored background and a gypsum bust in the foreground. Figure 2a shows the measured camera image when a constant gray image is projected. This resembles a coaxial bright-field illumination of the scene. Figure 2b shows the inverse illumination mask obtained by the feedback algorithm after 15 iterations. By projecting this image onto the scene, the camera measures a nearly constant gray image (Figure 2c). Figure 2d illustrates the *root mean square (RMS)* error [17] between the desired constant gray image $g_{target}(\mathbf{x}) = k$ and the actually measured camera image $g^t_{ms}(\mathbf{x})$ for each iteration t. The RMS error decreases rapidly and after approximately five iterations no further decrease of the RMS error is observable.

To evaluate the feasibility of the inverse illumination method for inspection tasks, the test scene is modified by small paper patches to simulate deviations from the desired nominal state of our scene. Then, the actual (modified) scene is illuminated by the inverse illumination mask of the nominal scene and an image is captured. The results are summarized in Figure 3. As expected, deviations from the nominal scene, which are simulated by colored paper patches, are clearly highlighted by the inverse illumination mask. Since deviations in reflectance and shape are directly displayed in the captured inspection image, the effort to detect these can be reduced. For instance, conventional image segmentation techniques based on color thresholding [17] may be used to identify the faulty regions in the inspection image (compare Figures 3e and 3f).

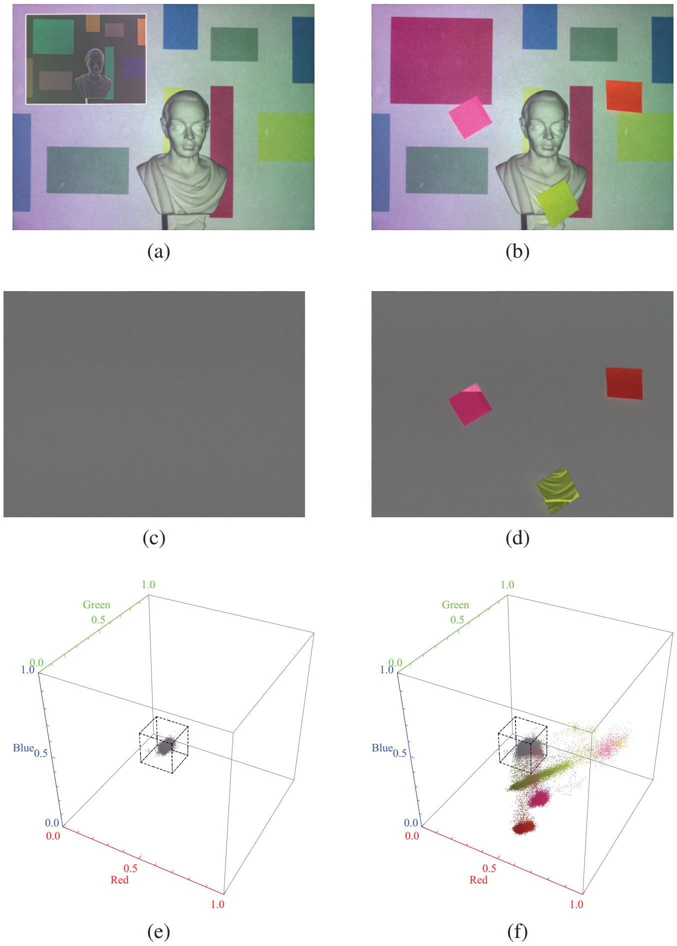

Fig. 3. Inverse illumination to highlight deviations from the desired nominal state of a test scene. (a) Nominal state of the scene with its inverse illumination mask shown as inset. (b) Modified scene by paper patches. (c) Original scene and (d) modified scene illuminated with the inverse illumination mask of the nominal state of the test scene. (e) Color distribution of the image pixels in Figure (c). Each image pixel corresponds to a vector in the RGB color space. The pixels are densely clustered and are enclosed by a bounding box which is centered on the color gray. (f) Color distribution of the image pixels in Figure (d). Points outside the bounding box belong to image regions that mark deviations from the nominal state of the scene.

Obviously, a similar result like in Figure 3c and 3d can be obtained by image differencing, which is a sensitive method for detecting intensity changes between coregistered images (compare Figure 4). In order to apply this technique for the detection of defects, the image differencing operation takes a reference image of the nominal scene and an image of the actual scene as input, where both images are captured under identical illumination conditions (e.g., under homogeneous bright-field illumination). The output is then a difference image whose pixel values are simply the differences of the corresponding pixel values from the two input images, with each color channel treated separately. Deviations from the reference image are then indicated by pixel values differing from zero. In the following Section IV, some theoretical considerations with regard to the signal-to-noise ratio of both techniques are presented.

IV. Comparison of Image differencing and Inverse Illumination for Deviation Detection

A. Model for Image-Signal Formation

To compare both techniques, the following simple signal model for the formation of a single-channel image $g(\mathbf{x})$ is considered, where spatially depending signals are denoted as functions of camera coordinates $\mathbf{x}$:

$$g(\mathbf{x}) = \rho(\mathbf{x})e(\mathbf{x}) + n(\mathbf{x}) \ . \tag{3}$$

Here $\rho(\mathbf{x})$ models the reflectance of a scene and $e(\mathbf{x})$ denotes the incident irradiance at an observed scene point $\mathbf{x}$ provided by the projector. Expression $n(\mathbf{x})$ is an additive noise signal with expected value $\mathrm{E}\{n(\mathbf{x})\} = 0$ and variance $\mathrm{Var}\{n(\mathbf{x})\} = \sigma_n^2(\mathbf{x})$, which comprises all additive camera noise sources.

Due to the quantum nature of light, another important noise component in image acquisition is photon shot noise, also referred to as Poisson noise, which arises from the counting statistics of the incident photons. The number of detected photons is subject to statistical fluctuations and obeys a Poisson distribution. To incorporate this illumination-depend noise component into the image signal model (3), the irradiance $e(\mathbf{x})$ is expressed in terms of the number of incident photons $\nu(\mathbf{x})$ and a conversion gain factor α which converters photon counts to irradiance units:

$$e(\mathbf{x}) = \alpha \cdot \nu(\mathbf{x}) \ . \tag{4}$$

As aforementioned, the number of photons $\nu(\mathbf{x})$ is a Poisson distributed random variable, and therefore $e(\mathbf{x})$ can be decomposed into a deterministic component $\bar{\nu}(\mathbf{x})$ and a stochastic noise component $\tilde{\nu}(\mathbf{x})$ according to

$$\begin{aligned} e(\mathbf{x}) &= \alpha\big(\underbrace{\nu(\mathbf{x}) - \mathrm{E}\{\nu(\mathbf{x})\}}_{=:\tilde{\nu}(\mathbf{x})} + \underbrace{\mathrm{E}\{\nu(\mathbf{x})\}}_{=:\bar{\nu}(\mathbf{x})}\big) \\ &= \alpha\big(\bar{\nu}(\mathbf{x}) + \tilde{\nu}(\mathbf{x})\big) \ . \end{aligned} \tag{5}$$

For obvious reasons, the noise signal has zero expected value $\mathrm{E}\{\tilde{\nu}(\mathbf{x})\} = 0$ and variance $\mathrm{Var}\{\tilde{\nu}(\mathbf{x})\} = \mathrm{Var}\{\nu(\mathbf{x})\}$. Since $\nu(\mathbf{x})$ obeys Poisson statistics, $\mathrm{Var}\{\nu(\mathbf{x})\} = \mathrm{E}\{\nu(\mathbf{x})\}$, and therefore the photon shot noise level $\mathrm{Var}\{\tilde{\nu}(\mathbf{x})\}$ equals the deterministic irradiance component $\bar{\nu}(\mathbf{x})$.

With (5), the image signal model (3) can be decomposed according to

$$g(\mathbf{x}) = \underbrace{\alpha\rho(\mathbf{x})\bar{\nu}(\mathbf{x})}_{=:S(\mathbf{x})} + \underbrace{\alpha\rho(\mathbf{x})\tilde{\nu}(\mathbf{x}) + n(\mathbf{x})}_{=:N(\mathbf{x})} \tag{6}$$

into the signal-of-interest $S(\mathbf{x})$ and a stochastic noise signal $N(\mathbf{x})$ that comprises the illumination-independent additive noise component $n(\mathbf{x})$ and the illumination-dependend multiplicative noise component $\alpha\rho(\mathbf{x})\tilde{\nu}(\mathbf{x})$. In the following, $n(\mathbf{x})$ and $\tilde{\nu}(\mathbf{x})$ are assumed to be mutually uncorrelated. Given the separation of $g(\mathbf{x})$ into signal-of-interest and noise, the *signal-to-noise ratio (SNR)* of $g(\mathbf{x})$ in $\mathbf{x}$ can be defined as follows:

$$\mathrm{SNR}(\mathbf{x}) := \frac{S(\mathbf{x})^2}{\mathrm{Var}\{N(\mathbf{x})\}} \ . \tag{7}$$

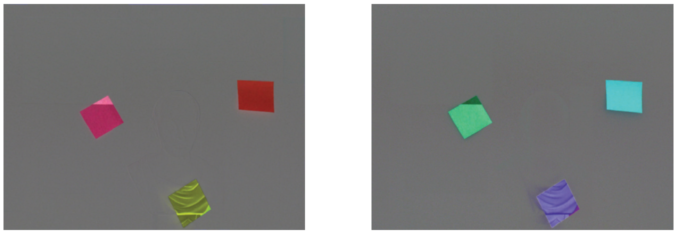

(a) (b)

Fig. 4. Inspection images obtained by inverse illumination (a) and image differencing (b). The difference image is obtained by subtracting the image of the modified scene in Figure 3b from the reference image of the nominal scene in Figure 3a and by adding an offset to avoid negative pixel values.

B. SNR of Difference Images

Based on the preceding considerations, the SNR of a difference image $g_D(\mathbf{x}) := g''(\mathbf{x}) - g'(\mathbf{x})$ can be derived in a similar fashion. For this purpose, two images

$$g'(\mathbf{x}) = \alpha\rho(\mathbf{x})(\bar{\nu}_D + \tilde{\nu}'_D) + n'(\mathbf{x}) \tag{8}$$

and

$$g''(\mathbf{x}) = \alpha \cdot (\rho(\mathbf{x}) + \Delta(\mathbf{x}))(\bar{\nu}_D + \tilde{\nu}''_D) + n''(\mathbf{x}) \tag{9}$$

are considered that differ in their reflectance function by the difference signal $\Delta(\mathbf{x})$, which models deviations in the observed scenes. Furthermore, it is assumed that both images are acquired under spatially homogeneous (and identical) illumination conditions, that is, the deterministic irradiance component $\bar{\nu}_D$ for acquiring $g'(\mathbf{x})$ and $g''(\mathbf{x})$ is constant and therefore the spatially dependency $\mathbf{x}$ is ignored. With (8) and (9), the difference image $g_D(\mathbf{x})$ becomes

$$\begin{aligned} g_D(\mathbf{x}) = & \underbrace{\alpha\rho(\mathbf{x})(\bar{\nu}_D - \bar{\nu}_D)}_{=0} + \underbrace{\alpha\bar{\nu}_D\Delta(\mathbf{x})}_{=:S_D(\mathbf{x})} \\ & + \underbrace{\alpha\tilde{\nu}'_D(\rho(\mathbf{x}) + \Delta(\mathbf{x})) - \alpha\tilde{\nu}''_D\rho(\mathbf{x}) + n'(\mathbf{x}) + n''(\mathbf{x})}_{=:N_D(\mathbf{x})}, \end{aligned} \tag{10}$$

where $S_D(\mathbf{x})$ is interpreted as the signal-of-interest and $N_D(\mathbf{x})$ is the noise signal. Consequently, according to (7), the SNR of $g_D(\mathbf{x})$ can be written, by defining and substituting $\sigma_D^2 := \mathrm{Var}\{\tilde{\nu}'_D\} = \mathrm{Var}\{\tilde{\nu}''_D\}$ and $\sigma_n^2(\mathbf{x}) := \mathrm{Var}\{n'(\mathbf{x})\} = \mathrm{Var}\{n''(\mathbf{x})\}$, as

$$\begin{aligned} \mathrm{SNR}_D(\mathbf{x}) = & \frac{\alpha^2\bar{\nu}_D^2\Delta(\mathbf{x})^2}{\alpha^2\sigma_D^2 \cdot (\rho(\mathbf{x}) + \Delta(\mathbf{x}))^2 + \alpha^2\sigma_D^2\rho(\mathbf{x})^2 + 2\sigma_n^2(\mathbf{x})} \\ \approx & \frac{\alpha^2\bar{\nu}_D^2\Delta(\mathbf{x})^2}{2\alpha^2\sigma_D^2\rho(\mathbf{x})^2 + 2\sigma_n(\mathbf{x})^2} \; . \end{aligned} \tag{11}$$

The approximation assumes $\Delta(\mathbf{x}) \ll \rho(\mathbf{x})$, i.e., the difference signal is much small compared to the reflectance of the scene.

C. SNR of Images Obtained by Inverse Illumination

As described in Section II, illuminating a scene by its inverse illumination mask yields a constant image $g_I(\mathbf{x})$ with a predefined constant gray value k, that is, $\mathrm{E}\{g_I(\mathbf{x})\} = k$. According to the signal model (6), the deterministic component of the incoming irradiance $\bar{\nu}_I(\mathbf{x})$ is then

$$\bar{\nu}_I(\mathbf{x}) = \frac{k}{\alpha\rho(\mathbf{x})} \; . \tag{12}$$

Let $\Delta(\mathbf{x})$ be again a difference signal to model small reflectance deviations from a predefined nominal state. Then the image signal by means of an inverse illumination can be written, by inserting (12) for $\bar{\nu}_I(\mathbf{x})$, as

$$\begin{aligned} g_I(\mathbf{x}) &= \alpha \cdot (\rho(\mathbf{x}) + \Delta(\mathbf{x}))(\bar{\nu}_I(\mathbf{x}) + \tilde{\nu}_I(\mathbf{x})) + n(\mathbf{x}) \\ &= k + \underbrace{k\frac{\Delta(\mathbf{x})}{\rho(\mathbf{x})}}_{=:S_I(\mathbf{x})} + \underbrace{\alpha\tilde{\nu}_I(\mathbf{x})(\rho(\mathbf{x}) + \Delta(\mathbf{x})) + n(\mathbf{x})}_{=:N_I(\mathbf{x})} \; , \end{aligned} \tag{13}$$

where $S_I(\mathbf{x})$ and $N_I(\mathbf{x})$ are interpreted as the signal-of-interest and the noise signal, respectively. Therefore, according to (7), the SNR of $g_I(\mathbf{x})$ can be written, by defining and substituting $\sigma_I^2(\mathbf{x}) := \mathrm{Var}\{\tilde{\nu}_I(\mathbf{x})\}$ and $\sigma_n^2(\mathbf{x}) := \mathrm{Var}\{n(\mathbf{x})\}$ as

$$\begin{aligned} \mathrm{SNR}_I(\mathbf{x}) = & \frac{k^2\Delta(\mathbf{x})^2\rho(\mathbf{x})^{-2}}{\alpha^2\sigma_I^2(\mathbf{x})(\rho(\mathbf{x}) + \Delta(\mathbf{x}))^2 + \sigma_n^2(\mathbf{x})} \\ \approx & \frac{k^2\Delta(\mathbf{x})^2}{\alpha^2\rho(\mathbf{x})^4\sigma_I^2(\mathbf{x}) + \rho(\mathbf{x})^2\sigma_n^2(\mathbf{x})} \; , \end{aligned} \tag{14}$$

where the approximation assumes $\Delta(\mathbf{x}) \ll \rho(\mathbf{x})$.

D. SNR Comparison of Image Differencing and Inverse Illumination

With the SNR as an objective quality measure defined for difference images and images obtained by inverse illumination, both techniques can be compared in a meaningful way. For this purpose, the *signal-to-noise ratio gain (SNRG)* is considered:

$$\begin{aligned} \mathrm{SNRG}(\mathbf{x}) := & \frac{\mathrm{SNR}_I(\mathbf{x})}{\mathrm{SNR}_D(\mathbf{x})} \\ = & \frac{2k^2(\alpha^2\sigma_D^2\rho(\mathbf{x})^2 + \sigma_n^2(\mathbf{x}))}{\alpha^2\bar{\nu}_D^2\rho(\mathbf{x})^2(\alpha^2\rho(\mathbf{x})^2\sigma_I^2(\mathbf{x}) + \sigma_n^2(\mathbf{x}))} \; . \end{aligned} \tag{15}$$

As indicated before, $\bar{\nu}_D$ and k denote parameters that control the image acquisition in both techniques and which both of them may be chosen freely. Since $\bar{\nu}_D$ sets the spatially homogeneous illumination condition for determining a difference image, a reasonable choice for $\bar{\nu}_D$ is

$$\bar{\nu}_D = \frac{g_{max}}{\alpha\rho_{max}} \; . \tag{16}$$

This ensures, that the highest reflectance value of a scene ρ_{max} is mapped to the maximal detectable gray value g_{max} and thus the whole range of gray values can be utilized. To set the parameter k, which controls the desired constant gray value for determining the inverse illumination mask, a similar argument leads to

$$k = \frac{g_{max}}{2} \; , \tag{17}$$

which ensures, that the difference signal $\Delta(\mathbf{x})$ is mapped to a wide range of gray values. With (16) and (17), $\bar{\nu}_D$ can be expressed in terms of k and ρ_{max}:

$$\bar{\nu}_D = \frac{2k}{\alpha\rho_{max}} \ . \tag{18}$$

To evaluate the SNR gain in (15), in the following two special cases are studied. In the presence of a great amount of light, that is, many photons are involved in the image formation process, the illumination-dependent noise components dominate the additive noise component, i.e., $\sigma_D^2 \gg \sigma_n^2(\mathbf{x})$ and $\sigma_I^2(\mathbf{x}) \gg \sigma_n^2(\mathbf{x})$. When the illumination-independent noise variance $\sigma_n^2(\mathbf{x})$ approaches zero, the SNR gain in high light conditions becomes

$$\mathrm{SNRG}_{high}(\mathbf{x}) = \frac{2k^2\sigma_D^2}{\alpha^2\bar{\nu}_D^2\rho(\mathbf{x})^2\sigma_I^2(\mathbf{x})} \ , \tag{19}$$

which can be further simplified by substituting $\sigma_D^2 = \bar{\nu}_D$ and $\sigma_I^2(\mathbf{x}) = \bar{\nu}_I(\mathbf{x}) = k^{-1}\alpha\rho(\mathbf{x})$, and by inserting (18) for $\bar{\nu}_D$, which then yields

$$\mathrm{SNRG}_{high}(\mathbf{x}) = \frac{\rho_{max}}{\rho(\mathbf{x})} \ . \tag{20}$$

Equation (20) shows that the SNR gain approaches infinity as the reflectance $\rho(\mathbf{x})$ approaches zero. This means, that the inverse illumination technique is particularly advantageous in dark scene region. In regions where $\rho(\mathbf{x})$ equals the highest scene reflectance ρ_{max}, image differencing and the inverse illumination technique perform equally well in SNR terms.

In the case of low light conditions, where are only few photons involved in the image formation process, the additive noise component dominates the illumination-dependent noise components, i.e., $\sigma_n^2(\mathbf{x}) \gg \sigma_D^2$ and $\sigma_n^2(\mathbf{x}) \gg \sigma_I^2(\mathbf{x})$. When σ_D^2 and $\sigma_I^2(\mathbf{x})$ approach zero, the SNR gain in low light conditions becomes

$$\mathrm{SNRG}_{low}(\mathbf{x}) = \frac{2k^2}{\alpha\bar{\nu}_D^2\rho(\mathbf{x})^2} \ , \tag{21}$$

which can be further simplified, by inserting (18) for $\bar{\nu}_D$, to:

$$\mathrm{SNRG}_{low}(\mathbf{x}) = \frac{\rho_{max}^2}{2\rho(\mathbf{x})^2} \ . \tag{22}$$

As in the case of a hight light level, the SNR gain approaches infinity as the reflectance $\rho(\mathbf{x})$ approaches zero, and therefore, the inverse illumination technique becomes particularly beneficial in dark scene regions. However, when the scene reflectance $\rho(\mathbf{x})$ approaches ρ_{max}, the SNR gain drops below one. Solving the equation

$$\frac{\rho_{max}^2}{2\rho(\mathbf{x})^2} = 1 \tag{23}$$

for $\rho(\mathbf{x})$ shows that the inverse illumination technique performs only better in terms of the SNR for scene reflectances $\rho(\mathbf{x}) < 2^{-\frac{1}{2}}\rho_{max}$.

V. Summary

An illumination technique that directly highlights deviations in reflectance between two scenes is proposed. This is achieved by generating an inverse illumination mask of the desired nominal state of the scene that "neutralizes" its appearance to a constant gray image. To compare the presented illumination technique with image differencing for deviation detection, for both techniques image-signal formation models are introduced and analyzed for their signal-to-noise ratios in low light and high light conditions. The evaluation of the comparison reveals, that especially in dark scene regions with low reflectance the proposed inverse illumination technique yields a positive gain in the signal-to-noise ratio.

In future works, we shall investigate the common principle and possible advantages of scene adapted illumination techniques more deeply and attempt to apply this principle to develop further novel illumination techniques.

References

[1] B. G. Batchelor and D. A. Hill, *Automated Visual Inspection*. Elsevier Science Publishing Company, Apr. 1985.

[2] J. E. Greivenkamp, *Field Guide to Geometrical Optics*. SPIE Society of Photo-Optical Instrumentation Engi, 2004.

[3] C. Steger, M. Ulrich, and C. Wiedemann, *Machine Vision Algorithms and Applications*, 1st ed. Wiley-Vch, Oct. 2007.

[4] W. Li, T. Bothe, W. Osten, and M. Kalms, "Object adapted pattern projection–Part I: generation of inverse patterns," *Optics and Lasers in Engineering*, vol. 41, no. 1, pp. 31–50, 2004.

[5] Y. Cai and X. Su, "Inverse projected-fringe technique based on multi projectors," *Optics and Lasers in Engineering*, vol. 45, no. 10, pp. 1028–1034, Oct. 2007.

[6] S. Werling and J. Beyerer, "Inspection of specular surfaces with inverse patterns," *tm-Technisches Messen*, vol. 74, no. 4, pp. 217–223, 2007.

[7] T. Baumbach, W. Osten, C. von Kopylow, and W. Jüptner, "Remote metrology by comparative digital holography," *Applied Optics*, vol. 45, no. 5, pp. 925–934, Feb. 2006.

[8] S. K. Nayar, H. Peri, M. D. Grossberg, and P. N. Belhumeur, "A projection system with radiometric compensation for screen imperfections," in *First IEEE International Workshop on Projector-Camera Systems (PROCAMS-2003)*, 2003.

[9] O. Bimber, D. Iwai, G. Wetzstein, and A. Grundhöfer, "The visual computing of projector-camera systems," *Computer Graphics Forum*, vol. 27, no. 8, pp. 2219–2245, 2008.

[10] R. Raskar, K. Low, and G. Welch, "Shader lamps: Animating real objects with Image-Based illumination," University of North Carolina at Chapel Hill, Tech. Rep., 2000.

[11] G. Garg, E. V. Talvala, M. Levoy, and H. P. Lensch, "Symmetric photography: Exploiting data-sparseness in reflectance fields," *Rendering Techniques*, pp. 251–262, 2006.

[12] G. Wetzstein and O. Bimber, "Radiometric compensation through inverse light transport," in *Proceedings of the 15th Pacific Conference on Computer Graphics and Applications*, 2007, pp. 391–399.

[13] M. Ashdown, T. Okabe, I. Sato, and Y. Sato, "Robust content-dependent photometric projector compensation," in *Conference on Computer Vision and Pattern Recognition Workshop*, 2006.

[14] K. Fujii, M. Grossberg, and S. Nayar, "A projector-camera system with real-time photometric adaptation for dynamic environments," in *IEEE Computer Society Conference on Computer Vision and Pattern Recognition CVPR*, vol. 1, 2005, pp. 814–821 vol. 1.

[15] M. Grossberg, H. Peri, S. Nayar, and P. Belhumeur, "Making one object look like another: controlling appearance using a projector-camera system," in *Proceedings of the 2004 IEEE Computer Society Conference onComputer Vision and Pattern Recognition CVPR*, vol. 1, 2004, pp. I–452–I–459 Vol.1.

[16] O. Bimber, A. Emmerling, and T. Klemmer, "Embedded entertainment with smart projectors," *Computer*, vol. 38, no. 1, pp. 48–55, 2005.

[17] R. C. Gonzalez and R. E. Woods, *Digital Image Processing*, 3rd ed. Prentice Hall International, Aug. 2008.